sustainability

MDPI

Article

Design and Implementation of an Integrated Sensor Network for Monitoring Abiotic Parameters During Composting

Abdulqader Ghaleb Naser [1,2], Nazmi Mat Nawi [2,3,*], Mohd Rafein Zakaria [3,4], Muhamad Saufi Mohd Kassim [2,3], Azimov Abdugani Mutalovich [5] and Muhammad Adib Mohd Nasir [2]

1 Department of Agricultural Machinery and Equipment, Faculty of Agriculture, Tikrit University, Tikrit 34001, Iraq; abdalkader.ghalib@gmail.com
2 Department of Biological & Agricultural Engineering, Faculty of Engineering, Universiti Putra Malaysia, Serdang 43400, Malaysia; saufi@upm.edu.my (M.S.M.K.); muhammadadib@upm.edu.my (M.A.M.N.)
3 Institute of Plantation Studies, Universiti Putra Malaysia, Serdang 43400, Malaysia
4 Department of Bioprocess Technology, Faculty of Biotechnology and Biomolecular Sciences, Universiti Putra Malaysia, Serdang 43400, Malaysia
5 Research Laboratory Innovative Water Treatment Systems, M. Auezov South Kazakhstan University, Taukehan Street 5, Shymkent 16000, Kazakhstan; azimov-78@mail.ru
* Correspondence: nazmimat@upm.edu.my; Tel.: +603-9769-4425

Abstract

Efficient composting is essential for sustainable organic waste management, yet conventional monitoring approaches are limited by single-parameter measurements and delayed response. This study presents an integrated sensor–AI framework designed to capture the interaction between thermal, chemical, and environmental factors governing composting. A distributed in-pile sensor network continuously measured temperature, moisture, and pH, while ambient parameters and gaseous emissions (O_2, CO_2, CH_4) were recorded to validate process dynamics. Statistical analyses, including correlation and regression modeling, were applied to quantify parameter interdependencies and the influence of external conditions. Results showed strong positive associations between temperature, moisture, and CO_2, and an inverse relationship with O_2, indicating active microbial respiration and accelerated decomposition. The validated sensors maintained high accuracy (±0.5 °C, ±3%, ±0.1 pH units) and supported real-time feedback control, leading to improved nutrient enrichment (notably N, P, and K) in the final compost. The framework demonstrates a transition from static measurement to intelligent, feedback-driven management, providing a scalable and reliable platform for optimizing compost quality and advancing sustainable waste-to-resource applications.

Keywords: composting; sensor technologies; machine learning models; real-time monitoring; nutrient enhancement

check for updates

Academic Editor: Giovanni De Feo

Received: 24 September 2025
Revised: 23 October 2025
Accepted: 28 October 2025
Published: 3 November 2025

Citation: Naser, A.G.; Nawi, N.M.; Zakaria, M.R.; Kassim, M.S.M.; Mutalovich, A.A.; Nasir, M.A.M. Design and Implementation of an Integrated Sensor Network for Monitoring Abiotic Parameters During Composting. *Sustainability* **2025**, *17*, 9780. https://doi.org/10.3390/su17219780

Copyright: © 2025 by the authors. Licensee MDPI, Basel, Switzerland. This article is an open access article distributed under the terms and conditions of the Creative Commons Attribution (CC BY) license (https://creativecommons.org/licenses/by/4.0/).

1. Introduction

Composting is a vital component for sustainable waste management, transforming organic residues into nutrient-rich amendment while reducing greenhouse gas emissions and supporting circular agriculture. Global organic waste volumes continue to rise, making an efficient composting process essential for maintaining soil health and mitigating the effects of climate change [1,2]. The performance of the composting process depends on controlling abiotic parameters—especially temperature, moisture, pH, and gaseous composition—that regulate microbial activity and decomposition rates. Thus, an accurate and responsive system capable of measuring multiple parameters in real time is needed by

the industry. However, most of the existing approaches remain fragmented or insufficiently validated at an operational scale.

Recent studies have reported monitoring systems that can improve parameter-specific monitoring. Ref. [3] developed a low-cost sensor assisted by machine learning platform for monitoring moisture content with excellent accuracy (r = 0.99). However, the system was not integrated with other critical variables. In another study, ref. [4] utilized photoacoustic sensors to detect CH_4 and N_2O at concentrations of 1 ppmv and 755 ppbv, respectively, without linking the gas data with process control. Ref. [5] proposed an electrochemical maturity sensor that incorporates pH, NH_4^+, and phosphatase activity, but requires extensive calibration for an actual application.

A wireless monitoring system was developed to track temperature and moisture variations in compost piles, though with limited process integration [6]. Several strategies have since been explored to improve composting performance. For example, automation technologies have shortened the bio-oxidation phase and increased yields [7], while amendments such as biochar have enhanced heat retention [8]. Laboratory-scale experiments have also demonstrated positive effects, including improved nitrogen retention [9] and greater weight reduction through controlled heating [10]. However, these approaches often require high infrastructure investment or controlled laboratory environments, making them difficult to implement in practical, large-scale composting operations. This limitation underscores the need for robust, field-ready integrated sensor systems explicitly designed for industrial composting applications.

Recent studies have demonstrated that machine learning can be utilized to predict composting parameters, including gas emissions and maturity, especially when large datasets are available. Random forest models have predicted CO_2 production with 88% accuracy [11] and metal bioavailability with a coefficient of determination (R^2) value of up to 0.97 [12]. Hyperspectral imaging combined with partial least squares regression (PLSR) enables non-destructive maturity assessment [13], while convolutional neural network (CNN) has achieved prediction accuracies of up to 96.4% [14]. Meta-learning has enhanced gaseous emission predictions [15], and XGBoost fusion models were utilized to facilitate automated food waste composting with high accuracy in predicting germination indices [16]. Despite high R^2 values reported across studies [17–19], challenges remain to develop a monitoring system with real-time integration.

In terms of microbial strategies, ref. [20] identified key microbial genera that influences decomposition, and ref. [21] optimized kitchen waste composting using machine learning, achieving a maturity score of 77.76%. Both studies highlighted that temperature and moisture control as critical factors for an effective composting process. Ref. [22] noted that differences in raw materials make it difficult to establish universal maturity indicators. The authors recommended rapid evaluation using machine learning, which requires robust multi-parameter datasets.

Recent commercial and experimental probes that integrate temperature, moisture, and pH sensing have also been used in controlled environments such as Agaricus bisporus cultivation and soil monitoring [3–6]. However, these systems are generally optimized for stable microclimates and short-term laboratory trials, with limited adaptability to heterogeneous, large-scale compost piles. Their calibration stability is often restricted, and long-range data transmission or real-time threshold control is rarely implemented. In contrast, the present study introduces a modular and wireless sensing framework specifically validated under tropical open-field conditions, combining embedded calibration, statistical verification, and cloud-ready data acquisition. This approach extends the functionality of existing integrated probes by enabling continuous, field-scale monitoring suitable for operational composting management.

The novelty of the present system lies in its integration of multiple technical and methodological features rarely combined in previous studies. Unlike earlier compost or soil probes that measure isolated parameters or operate under controlled laboratory settings [3–6], this framework employs synchronized multi-depth sensing of temperature, moisture, and pH with embedded real-time calibration and wireless data transmission. The modular architecture based on the ATmega2560 platform enables scalable deployment across large windrows while maintaining high measurement precision (±0.5 °C, ±3%, ±0.1 pH units) under fluctuating tropical conditions. Moreover, the incorporation of statistical validation and cloud-compatible data formatting allows direct coupling with AI-driven analytical models for predictive process control. This combination of low-cost hardware, validated field operation, and intelligent data integration represents a distinct advancement over previously reported systems, bridging the gap between laboratory prototypes and fully functional, real-world compost monitoring networks.

Taken together, the literature reveals three persistent gaps: (i) fragmented monitoring of single parameter which leads to a limited understanding of interactive effect on microbial dynamic; (ii) insufficient field-scale validation of advanced monitoring and modeling approaches; and (iii) lack of universally recognized maturity indicators to support standardization across composting systems. This study addresses these gaps through four contributions. First, it presents an integrated sensing platform capable of continuously monitoring the temperature, moisture, and pH, thereby overcoming the fragmentation of single-parameter systems. Second, it provides full-scale field validation under operational composting conditions. Third, it establishes a standardized, reproducible dataset for core abiotic parameters, enabling cross-site comparison and supporting future adoption of universal maturity metrics. Finally, by generating continuous, structured data stream, it enables direct integration with machine learning models for predictive control, offering a scalable framework adaptable by the relevant industry.

2. Materials and Methods

2.1. Experimental Setting and Pile Design

The experiment was conducted at Universiti Putra Malaysia (UPM), PUTRA Agricultural Center, Serdang, Selangor, Malaysia (2°59′16.0″N, 101°42′22.9″E), located in a lowland tropical rainforest climate characterized by heavy annual rainfall (>2500 mm) and consistently elevated temperature (24–33 °C). These conditions accelerate microbial decomposition, but also complicate composting management due to rapid fluctuations in moisture and heat loss. To represent typical tropical field condition, the trial was conducted from June to December 2022, ensuring exposure to seasonally warm and humid weather. The study aimed to evaluate compost maturity while validating an integrated multi-parameter sensing system under operational windrow condition. Three compost piles of varying sizes and compositions were constructed (Figure 1), each incorporating different proportions of green residues, yellow leaves, sawdust, horse waste, and sludge water (Tables 1–3). The choice of substrates reflected locally available materials, thereby enhancing practical relevance. To ensure botanical diversity, yellow leaves included equal proportions of *Ficus benghalensis*, *Swietenia macrophylla*, and *Mangifera indica*, while green residues comprised *Paspalum conjugatum*, *Axonopus compressus*, and *Bidens pilosa*.



Figure 1. Preparation of the compost piles.

Table 1. Physical properties of the compost piles.

Pile	Length (m)	Radius (m)	Volume (m^3)	Total Weight (kg)
1	10	1.00	14.2	5000
2	10	0.55	4.75	3200
3	13	0.80	14.1	5000

Table 2. Compositional properties of the compost piles.

Pile	Green Material		Yellow Leaves		Sawdust		Horse Waste		Sludge Water	
	(kg)	(%)	(kg)	(%)	(kg)	(%)	(kg)	(%)	(kg)	(%)
1	625	13	675	13	1200	24	1670	33	830	17
2	0	0	576	18	1024	32	1067	33	533	17
3	1250	25	450	9	800	16	1670	33	830	17

Table 3. Physicochemical characteristics of the feedstock materials used in composting.

Material	Total C (%)	Total N (%)	C/N Ratio	Lignocellulose (%)	pH (1:5)	Remarks/Function
Green residues	52.7	2.85	18.5	Cellulose 22.4; Lignin 16.2	6.5	Nitrogen source, rapid decomposer
Yellow leaves	58.0	1.61	36.1	Cellulose 25.8; Lignin 28.1	6.4	Carbon source, moderate decomposition
Sawdust	64.8	0.79	82.4	Cellulose 20.5; Lignin 31.0	6.9	Bulking agent, aeration support
Horse waste	54.2	2.14	25.3	Cellulose 18.3; Lignin 12.6	7.4	Organic matter + microbial inoculum
Sludge water	32.1	2.58	12.4	Low solid content	7.1	Moisture and soluble nutrients

The physicochemical composition of the feedstock materials was analyzed prior to pile construction to establish their baseline carbon and nutrient properties. Representative samples of each component were oven-dried at 70 °C and ground to pass a 2 mm sieve. Total carbon (C) and nitrogen (N) were determined by dry combustion, lignocellulose fractions (cellulose, hemicellulose, and lignin) by Van Soest sequential fiber analysis, and pH in a 1:5 w/v aqueous suspension. The results (Table 3) indicated that the green residues possessed a high nitrogen content (2.9%) and a moderate C/N ratio (18.5), reflecting their protein-rich nature, while the yellow leaves exhibited higher lignocellulose fractions (lignin 28%) and a C/N ratio of 36.1, representing a slow-degrading carbon source. Sawdust

showed the highest lignin proportion (31%) and a very wide C/N ratio (82.4), serving as a bulking and structural amendment. Horse waste provided both organic matter and additional microbial inoculum, with a C/N ratio of 25.3, whereas the sludge water contributed soluble nutrients and moisture adjustment (C/N ≈ 12.4, pH 7.1). The balanced combination of these materials ensured a composite feedstock with an initial overall C/N ratio near 30, which is favorable for microbial activity and thermophilic phase initiation.

The quantities and proportions of the components in the three compost piles (Tables 2 and 3) were established based on the target carbon-to-nitrogen ratio (25–30:1) and moisture content (55–60%), ensuring a balanced supply of degradable carbon and nitrogen sources [3,6]. Green residues served as a rapid nitrogen source, yellow leaves and sawdust provided structural carbon and improved aeration, horse manure contributed microbial inoculum and organic enrichment, and sludge water maintained optimal moisture and soluble nutrient content. The ratios represented various substrate compositions for performance comparison under controlled conditions.

Advanced embedded sensors continuously monitored temperature, moisture, and pH, enabling data-driven management. Interventions such as watering and turning were triggered when thresholds were exceeded, following scientifically established guidelines [23,24]. These thresholds (Table 4) targeted thermophilic stability (50–70 °C), aerobic moisture levels (40–60%), and a favorable pH range (4.2–7.2) for the compost piles. By combining varied pile compositions with sensor-guided management, the design established both controlled and heterogeneous conditions. This structured preparation provided a rigorous framework to assess the reliability of real-time monitoring systems in optimizing compost maturity and quality under tropical field conditions.

Table 4. Thresholds for the compost pile management interventions.

Parameter	Threshold Condition	Action	Scientific Rationale
Temperature (°C)	<50 or >70	Turning and watering	Aerates pile, maintains moisture, prevents overheating; aligns with optimal thermophilic range
	50–70	No action	Favorable for rapid microbial degradation
Moisture (%)	<40	Watering	Prevents microbial inactivity due to desiccation
	40–60	No action	Ideal for sustaining aerobic microbial processes
	>60	Turning	Prevents anaerobic conditions by increasing aeration
pH	<4.2	Watering	Buffers acidity, supports microbial community balance
	4.2–7.2	No action	Optimal range for microbial activity and nutrient retention
	>7.2	Turning and watering	Reduces ammonia volatilization and excessive alkalinity

2.2. Sensor Placement and Data Collection

To address the spatial heterogeneity inherent in windrow composting, a structured sampling framework was established using a custom auger-mounted platform for precise sensor positioning (Figure 1). Each cluster integrated a temperature probe, a capacitive moisture sensor, and a pH electrode (Section 2.4), aligned adjacently to capture co-located measurements from the same microenvironment. By ensuring synchronized readings across parameters, temporal comparability was maintained, which is critical for process validation and multivariable interpretation. Along the pile length, sampling points were spaced at 1.0 m intervals to optimize spatial resolution while preserving operational feasibility. At each horizontal point, measurements were taken at three depths (core, middle, and surface), with three replicate readings taken at each depth. Vertical stratification was applied by sampling the composting piles at three depths; the core (0.75–1.0 m from the top surface), the middle (~0.5 m), and the surface (~0.1–0.2 m). These depths were chosen based on

the established recommendations [2], reflecting distinct microclimatic zones that govern microbial metabolism, aeration, and water retention.

This produced nine readings per point, which were averaged to generate depth-specific values and then integrated into comprehensive spatial profiles (Table 5). Measurements were conducted every three days at consistent time to minimize diurnal variability. This schedule generated an extensive dataset that captured both temporal and spatial dynamics of temperature, moisture, and pH. The resulting protocol, summarized in Table 5, yielded 90 to 117 readings per measurement depending on the pile length. Such systematic coverage enabled robust evaluation of sensor performance across both vertical and longitudinal gradients, ensuring that assessment reflected realistic heterogeneity in operational composting environments. This foundation directly supports subsequent analyses of sensor accuracy and composting process dynamic under tropical field conditions.

Table 5. Sampling protocol for the compost piles.

Parameter	Pile 1	Pile 2	Pile 3
No. of sample	3 (core, middle, surface)	3 (core, middle, surface)	3 (core, middle, surface)
Depths from the surface (m)	0.75–1.0, ~0.5, 0.1–0.2	0.75–1.0, ~0.5, 0.1–0.2	0.75–1.0, ~0.5, 0.1–0.2
Number of horizontal points	10	10	13
Replicates per depth point	3	3	3
Readings per point	9	9	9
Total readings/event	90	90	117

2.3. Integrated and Modular Framework for the Compost Monitoring and Control

To advance beyond conventional compost monitoring practice, a custom-built, fully integrated system was developed to deliver continuous, real-time tracking of key abiotic parameters. Unlike traditional setups that rely on separate instruments, this system consolidated temperature, moisture, and pH sensing within a single cluster, thereby enhancing data comparability and reducing operational complexity. Each pile was equipped with a DS18B20 digital temperature probe, a capacitive soil moisture sensor, and an analog pH electrode, all of which were selected for their robustness and accuracy in high-moisture and organic environments. These sensors interfaced with an ATmega2560 microcontroller, whose RISC-based architecture, extensive I/O capacity, and embedded calibration functions which enabled real-time signal conversion into engineering units. Sensor outputs were displayed on a two-line I^2C LCD for immediate field feedback and logged to a microSD card, ensuring redundant long-term storage in the event of wireless transmission failure.

Wireless communication was facilitated by nRF24L01 transceiver operating at 2.4 GHz, chosen for its low power consumption and reliability under field conditions. The transmitted data were received, decoded, and automatically validated before being integrated into a centralized data acquisition (DAQ) framework. This modular design enabled scalable coordination across multiple microcontrollers and heterogeneous sensors, extending beyond basic environmental measurement to include laser-based pile dimension assessments and rotary encoder inputs for monitoring platform movement. Optimized signal processing protocols were applied—pH readings stabilized via median filtering, temperature acquired through OneWire protocols, and soil moisture converted from analog to digital signals using calibrated functions—thereby ensuring measurement accuracy.

Figure 2 illustrates the integrated architecture of data flow, control logic, and modular expansion within the monitoring framework. The workflow encompassed two operational phases: initialization of sensors, variables, and wireless modules, followed by continuous acquisition, processing, display, logging, and wireless transfer. Data routed to the DAQ unit was reformatted for seamless integration with cloud-based analytical tools, enabling structured storage, secure access, and subsequent machine learning application. By linking

low-level sensing with advanced analytics, the system established a closed-loop monitoring framework in which real-time comparisons against management thresholds supported timely interventions, such as turning or watering. Collectively, this approach enhanced the efficiency of composting operation, improved compost quality, and increased the overall reliability of tropical composting systems.

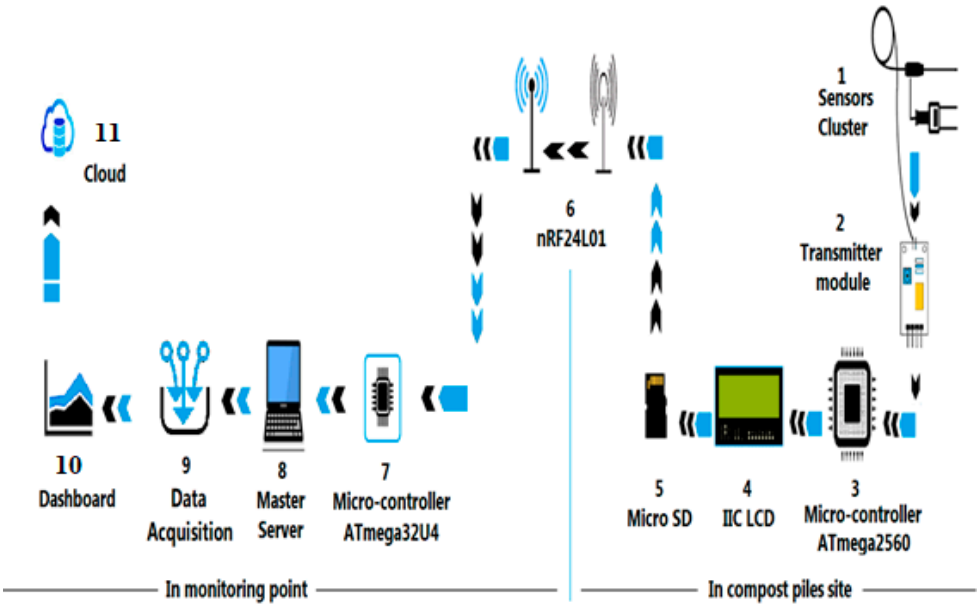


Figure 2. System architecture for real-time compost monitoring and control.

The integrated sensor framework was coupled with a data analytics module designed to support machine learning-based prediction and control. Real-time temperature, moisture, and pH readings were normalized using min–max scaling (Equation (5)) and wirelessly transmitted to the data acquisition (DAQ) unit, where each entry was time-stamped, geo-tagged by pile ID and depth, and merged with ambient parameters (O_2, CO_2, CH_4, humidity, and temperature). This produced a structured dataset for multivariate modeling. Supervised algorithms, including multiple linear regression and random forest regression, were implemented in MATLAB R2023b to predict thermophilic duration, moisture depletion, and compost maturity status. Data were divided into 80% training and 20% testing subsets, with five-fold cross-validation to ensure robustness. Model performance was evaluated using R^2, RMSE, and MAE indices. The predictive outputs were linked to a decision rule module that could recommend aeration or watering actions when predicted values exceeded defined thresholds. This integration establishes a real-time feedback loop between sensing, analytics, and management, transforming the system from passive data collection into an adaptive, AI-assisted platform capable of optimizing composting efficiency under varying environmental and feedstock conditions.

2.4. Sensor Deployment and Functional Performance

Accurate monitoring of compost abiotic condition was achieved through the deployment of three calibrated sensor types: DS18B20 digital temperature sensors, capacitive moisture sensors, and glass electrode pH sensors (Table 6). These devices were chosen for their balance of accuracy, affordability, and proven applicability in compost and soil environment [25,26]. Their combined functionality enabled continuous detection of critical process shifts that influence microbial activity and compost quality.

Table 6. Specifications and deployment of the monitoring sensors.

Parameter	Sensor Type	Principle of Measurement	Range	Accuracy/ Resolution	Output Signal	Interface to ATmega2560	Deployment Details
Temperature	DS18B20 (digital)	Semiconductor-based thermal sensing	−55 to 125 °C	±0.5 °C/ 0.0625 °C	Digital (1-Wire)	Direct digital input	Inserted at 3 depths per pile, PVC-cased
Moisture	Capacitive sensor	Dielectric permittivity of compost	0–100% VWC	±3%/10-bit ADC step	Analog voltage	ADC (10-bit)	Replicated at each depth, recalibrated monthly
pH	Glass electrode	Voltage from H+ ion exchange	3.0–14.0 pH	±0.1 pH	Analog voltage	ADC (10-bit)	Weekly calibration with buffer standards

(Sensor models and sources: DS18B20 Digital Thermometer—DFRobot Industries, Available online: https://www.dfrobot.com/product-1354.html (accessed on 1 March 2022); Capacitive Soil Moisture Sensor v1.2—DFRobot, China; Available online: https://www.dfrobot.com/product-2054.html (accessed on 1 March 2022); Gravity: Analog pH Sensor Kit—Atlas Scientific, USA, Available online: https://www.atlas-scientific.com/ (accessed on 1 March 2022).

The DS18B20 temperature sensor, operating on a 1-Wire protocol, offered ±0.5 °C accuracy within a −55 to 125 °C range, with a 12-bit resolution (0.0625 °C). This precision was essential for identifying mesophilic and thermophilic phases, which serve as benchmarks for compost maturity. Complementing this, the capacitive moisture sensor quantified volumetric water content (0–100% VWC) by measuring changes in dielectric permittivity. Its corrosion-resistant design and ±3% accuracy made it reliable under the saline and humid conditions typical of compost piles, allowing detection of both water deficits and excesses linked to microbial inhibition and anaerobiosis. Meanwhile, the glass electrode pH sensor, which covers a range of 3.0–10.0 with a precision of ±0.1 units, captured shifts associated with ammonification and organic acid formation, two key biochemical processes involved in organic matter stabilization.

The developed system was designed with affordability and industrial adaptability as primary considerations. The total hardware cost per unit—including temperature, moisture, and pH sensors; wireless transceiver; data-logging microcontroller; and protective housing—was approximately USD 250, significantly lower than the price of comparable commercial probes. All components were enclosed in IP65-rated casings and tested for thermal endurance up to 70 °C and 95% relative humidity, ensuring long-term durability under composting conditions. The modular design allows up to 20 nodes to be connected to a single gateway through a mesh communication topology, enabling scalable deployment across large windrows or multiple composting bays. Maintenance requirements are minimal, limited mainly to periodic calibration checks and battery replacement every 3–4 months. The combination of low cost, environmental resilience, and flexible scalability demonstrates that the proposed system can be readily adapted for real-world industrial composting operations, supporting both centralized monitoring and distributed process optimization.

Deployment was standardized across piles, with sensors inserted at three depths (surface, middle, and core) and replicated thrice per pile (Section 2.2). Each device was enclosed in PVC casings to mitigate compaction and leachate damage. Data processing included embedded moving-average filtering and calibration corrections (Section 2.5, Equations (1)–(4)), supported by periodic recalibration. Together, these protocols ensured data accuracy, minimized sensor drift, and provided robust, continuous measurements under field conditions.

2.5. Calibration Protocol for the Compost Monitoring Sensors

To ensure precise and reliable measurement of the composting parameters, a rigorous multi-stage calibration protocol was established for the moisture, temperature, and pH sensors, integrating laboratory reference methods with the field validation. This approach

was designed to reduce systematic bias, improve reproducibility, and meet environmental monitoring standards [27,28]. Figure 3 and Table 7 summarize the calibration process and outcomes.

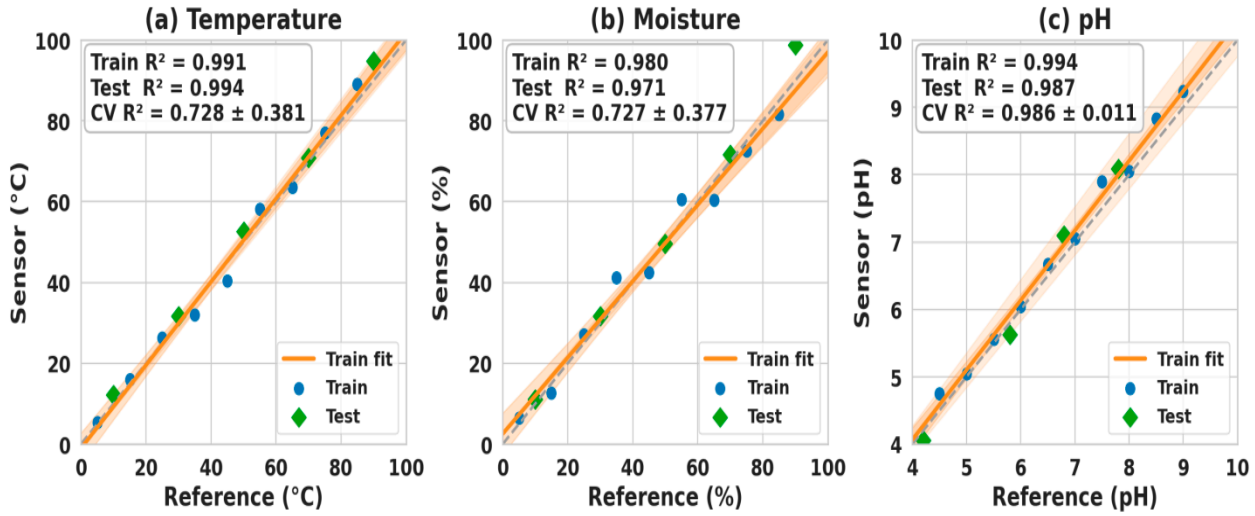


Figure 3. Validation plots for temperature, moisture, and pH sensors. Train points (blue) were used to fit the calibration line, while test points (green) were used for validation; the orange line shows the fit with 95% confidence intervals.

Table 7. Calibration performance of the compost monitoring sensors.

Sensor Type	Slope (mm)	Intercept (bb)	R^2	Mean Absolute Error (MAE)	Max Error	Min Error	Standard Deviation
Moisture	1.015	0.82	0.984	2.83%	3.40%	0.30%	1.75%
Temperature	0.998	0.12	0.998	0.20 °C	1.00 °C	−0.50 °C	0.53 °C
pH	1.003	−0.05	0.996	0.04 pH units	0.08	0.00	0.03

Moisture calibration employed the gravimetric oven-drying method, in which samples were dried at 70 °C for a period of three days. Actual moisture content was calculated using Equation (1), and sensor voltage outputs were linearly regressed against reference values (Equations (2) and (3)). This yielded a mean absolute error (MAE) of 2.83% (SD = 1.75%), with R^2 = 0.984, demonstrating high predictive accuracy. Temperature calibration followed a three-point reference scheme using ice water (0 °C), ambient (~25 °C), and boiling water (100 °C), supplemented by intermediate checks at 50 °C and 75 °C. Regression fitting (Equation (4)) yielded an average deviation of 0.20 °C, with an R^2 value of 0.998, confirming its suitability for identifying thermophilic and mesophilic phases. pH calibration followed the American Public Health Association (APHA) Standard Methods for the Examination of Water and Wastewater (2017), using buffer solutions at pH 4.00, 7.00, and 10.00. Two-point adjustments were embedded into firmware to correct for slope and offset drift, yielding an R^2 of 0.996 and a maximum error of 0.1 units. Finally, independent validation using portable field sensors confirmed strong agreement with fixed in-pile devices (Pearson's $r > 0.95$). Embedding calibration Equations (1)–(4) into the firmware ensured operational robustness, statistical validation, and high-fidelity data streams, which are essential for automated compost process control.

$$Actual\ Moisture\ Content(\%) = \frac{Wi - Wd}{Wd} \times 100 \quad (1)$$

where Wi is the initial (wet) weight, and Wd is the oven-dry weight.

Sensor voltage outputs (y) were plotted against actual moisture content (x), and a linear regression was fitted to derive the calibration equation:

$$y = mx + b \quad (2)$$

where m is the slope (sensor sensitivity), and b is the intercept (systematic offset). For microcontroller integration, the inverse form was applied to convert raw readings into moisture content:

$$x = \frac{y - b}{m} \quad (3)$$

$$Tsensor = m \times Treference + b \quad (4)$$

where m was the slope, and b was the y-intercept.

2.6. Validation Protocols for Sensor Accuracy

Ensuring long-term stability and accuracy of the sensors in the compost environments required a rigorous calibration–validation framework designed to mitigate drift, biofilm formation, and fluctuating abiotic conditions [26,29]. While laboratory calibration established baseline accuracy (Section 2.5), systematic field validation against precision instrument ensured sustained reliability over the 12-week experimental period. Validation was performed weekly across three compost piles, with readings taken at three depths (core, middle, and surface) and three replicates per depth, generating 27 paired measurements per week for each parameter. This design yielded 324 validation points per sensor type. For validation, temperature readings from the DS18B20 digital sensor were cross-checked against measurements obtained using the thermocouple probe included in the Agriculture Soil Test Kit (SMT100-TRUEBNER GmbH, Neustadt, Germany, 2022), which is rated for temperatures up to 85 °C and designed for semi-solid materials such as compost. Meanwhile, soil moisture values were validated using the same kit (SMT100-TRUEBNER GmbH, Neustadt, Germany, 2022), following gravimetric calibration in the laboratory to ensure high measurement accuracy and consistency across sensors (Table 8). pH measurements from the integrated sensor system were validated against a Bluelab Soil pH Pen (Bluelab Corporation Limited, Tauranga, New Zealand) (Table 9).

Table 8. Specifications of the integrated soil testers used in the compost monitoring.

Specifications	Value
SMT100-TRUEBNER GmbH-Germany	TRUEBNER GmbH (Neustadt, Germany, 1 March 2022). Available online: https://ictinternational.com/product/smt-100-soil-moisture-and-soil-temperature-probe/ (accessed on 1 March 2022)
Moisture range	0–100 % VWC
Temperature range	–20 to +85 °C
Interfaces/outputs	RS-485 (ASCII/Modbus/T-Bus)
Power & protection	Supply 4.0–28 V DC
Moisture accuracy	±3 % VWC
Temperature accuracy	Typical ±0.2 °C
Measured parameters	Volumetric water content & soil temperature
SMT100-TRUEBNER GmbH-Germany	https://ictinternational.com/product/smt-100-soil-moisture-and-soil-temperature-probe/ (accessed on 1 March 2022)

Table 9. Specifications of the portable soil pH tester used in the compost monitoring.

Specifications	Value
Model	Bluelab Soil pH Pen (Bluelab Corporation Limited, 2021, New Zealand). Available online: https://bluelab.com/products/bluelab-soil-ph-pen (accessed on 1 March 2022)
Measurement Resolution	0.1 pH, 1 °C/1 °F
Measurement Range	0.0–14.0pH, 0–100 °C
Measurement Accuracy	±0.1 pH, ±1 °C/±2 °F
Calibration Requirement	Two-point (pH 7.0 & 4.0 or 10.0)
CE/FCC/RoHS Compliance	Yes
Automatic Temperature Compensation	Yes

Statistical analysis included regression-derived slope, intercept, and R^2, supplemented by root mean square error (RMSE), mean absolute error (MAE), and mean absolute percentage error (MAPE) indices. Bias and 95% confidence intervals quantified systematic deviations. Results (Table 10) confirmed excellent agreement, with R^2 values exceeding 0.99 across all sensors, and narrow errors: RMSE of 0.35 °C, 1.42% moisture, and 0.08 pH units. Regression plots (Figure 3) further illustrated alignment with the 1:1 reference line. Notably, these tolerances were markedly lower than the typical error ranges reported for uncalibrated low-cost sensors, which often drift by more than 5% in moisture or ±1–2 °C in temperature under field conditions [25,30]. By linking validated measurements directly to the control interventions (Table 4), the framework safeguarded against false triggers, ensuring operational efficiency. Collectively, the integration of calibration, weekly validation, and process-based deployment established a robust pipeline that exceeded standard performance benchmarks and delivered defensible data streams for optimizing the compost process.

Table 10. Validation performance of the compost monitoring sensors.

Sensor Type	Slope (m)	Intercept (b)	R^2	RMSE	MAE	MAPE	Bias (±95% CI)
Temperature (°C)	0.99	+0.12	0.998	0.35 °C	0.27 °C	0.62%	+0.05 ± 0.21
Moisture (%)	0.97	+0.84	0.994	1.42%	1.05%	2.11%	−0.12 ± 0.64
pH	1.01	−0.03	0.991	0.08	0.06	1.05%	+0.02 ± 0.04

2.7. Environmental Profiling and Emission Assessment

Accurate characterization of external environmental conditions and gaseous outputs was essential for contextualizing composting dynamics and validating the in-pile sensor performance. Ambient temperature was continuously logged using a digital thermo-hygrometer (Testo 174H, Testo SE & Co. KGaA, Titisee-Neustadt, Germany), positioned approximately one meter above the windrows under shaded but ventilated conditions to minimize direct solar heating. Measurements were recorded at 30 min intervals, subsequently averaged into 24 h means, thereby capturing diurnal fluctuations relevant to microbial activity and pile thermodynamics. In parallel, gaseous emissions of O_2, CO_2, and CH_4 were quantified using a portable multi-gas analyzer (Geotech GA5000, QED Environmental Systems, Birmingham, UK). This instrument utilized infrared absorption for CO_2 and CH_4 detection, as well as electrochemical sensing for O_2. The stainless-steel probes were inserted at 0.5 m, 1.0 m, and 1.5 m depths to sample the pile core. To avoid transient sampling artifacts, each measurement was stabilized for approximately two minutes before recording. Readings were collected twice daily, morning and afternoon, and were cross-referenced with ambient air baselines to ensure accuracy and minimize drift.

Additionally, weekly volume assessments were conducted to monitor mass reduction and density changes. Pile height and base radius were measured at three equidistant points using a laser distance meter and calibrated tape. These values informed a composite geometric model combining trapezoidal prism and conical frustum equations [25,26]. Replicated across three piles, this protocol minimized error while revealing temporal declines in biomass. Finally, synchronization of ambient, gaseous, and volumetric data streams with the in-pile sensor outputs enabled integrated correlation and regression analyses, thereby strengthening the reliability of subsequent statistical modeling in Sections 3.5 and 3.6. Unlike many compost monitoring studies that rely solely on surface or weekly ambient measurements, this approach ensured high-frequency, multi-depth, and geometrically validated environmental profiling.

2.8. Laboratory Analytical Methods for Nutrient and C:N Ratio Evaluation

The compost nutrient composition was determined using the internationally recognized standards in ISO/IEC 17025–accredited and institutional laboratories (ERAS Laboratory, Malaysia). The analyses targeted major and trace nutrients, along with organic carbon, to support the accurate calculation of the carbon-to-nitrogen (C:N) ratio, a key indicator of the compost maturity.

Analytical protocols followed the guidelines of the Association of Official Analytical Chemists (AOAC), the International Organization for Standardization (ISO), and the United States Environmental Protection Agency (EPA). Total nitrogen and organic carbon were determined by dry combustion using an Elemental Analyzer [31–33], while phosphorus, potassium, magnesium, calcium, boron, sulfur, and trace metals were quantified by Inductively Coupled Plasma–Optical Emission Spectrometry (ICP-OES) following acid digestion [34–36]. Results were reported either as percentages of dry matter for macronutrients and carbon, or as parts per million (ppm) for micronutrients. A summary of the analytical protocols and corresponding standard references is provided in Table 11. These methods ensured the reliable quantification of the compost's macro and micronutrient availability, while compliance with AOAC, ISO, and EPA standards reinforced the analytical quality. The results provided the basis for evaluating compost quality and maturity, as presented in the Section 3.

Table 11. Laboratory methods for measuring the compost nutrient and C: N ratio.

Parameter(s)	Instrument/Method	Reporting Unit	Standard Reference
Nitrogen (N)	Elemental Analyzer, dry combustion	% dry matter	[32]
Carbon (C)	Elemental Analyzer, dry combustion	% dry matter	[31,33]
P_2O_5, K_2O, MgO, CaO	ICP-OES after acid digestion	% dry matter	[34]
B_2O_3, Zn, Fe, Cu, Mn	ICP-OES after acid digestion	ppm	[35,36]
Sulfur (S)	ICP-OES after acid digestion	% dry weight	[34]

3. Results

3.1. Statistical Validation of the Sensor Accuracy in Compost Monitoring Using ANOVA

The reliability of the sensor-based compost monitoring was rigorously evaluated using one-way analysis of variance (ANOVA), comparing the temperature, moisture, and pH measurements from the developed system with those from the reference instruments. Validation spanned all composting phases—mesophilic, thermophilic, cooling, and maturation—thereby testing the sensor performance under dynamic physicochemical conditions.

Table 12 summarizes the ANOVA results, indicating that there are no statistically significant differences between sensor and reference measurements for temperature, moisture, or pH, with all p-values greater than 0.05 (temperature: $F(3,116) = 1.42$, $p = 0.24$, $\eta^2 = 0.02$;

moisture: F(3,116) = 1.88, $p = 0.14$, $\eta^2 = 0.03$; pH: F(3,116) = 2.01, $p = 0.11$, $\eta^2 = 0.03$). Effect sizes were consistently small ($\eta^2 < 0.05$), and confidence intervals for mean differences overlapped zero, reinforcing statistical equivalence. Post hoc Tukey's HSD tests confirmed that no composting phase exhibited significant divergence. Minor variance during the thermophilic stage, particularly in terms of moisture, reflected rapid microbial-driven water loss rather than a systematic bias. Importantly, all observed deviations remained within narrow agronomic tolerances (±3% for moisture, ±0.5 °C for temperature, and ±0.1 pH units), confirming that the sensor outputs were equivalent to those of their reference instruments.

Table 12. ANOVA results for the sensor validation across the composting phases.

Parameter	Reference Device	F (df)	*p*-Value	η^2 (Effect Size)	95% CI (Mean Difference)	Post Hoc Tukey's Outcome	Agronomic Error Range
Temperature	Integrated soil tester	1.42 (3,116)	0.24	0.02	−0.40 to +0.30 °C	No sig. difference	±0.5 °C
Moisture	Integrated soil tester	1.88 (3,116)	0.14	0.03	−2.8% to +2.1%	No sig. difference	±3%
pH	Bluelab pH pen	2.01 (3,116)	0.11	0.03	−0.15 to +0.10	No sig. difference	±0.1 units

These validated error levels were less than half of the >5% drift commonly reported for uncalibrated low-cost sensors in compost environments [26,29]. These results demonstrate that the calibration–validation pipeline (Sections 2.5–2.7) effectively safeguarded sensor accuracy throughout the composting process. By reducing errors to below 50% of typical drift levels, this study provides statistically grounded evidence that low-cost sensors, when rigorously validated, can achieve accuracy suitable for both operational process control and scientific research.

3.2. Comprehensive Validation of the Sensor Technology

A two-way ANOVA was applied to validate the sensor performance across the composting phases while benchmarking against the reference instruments, thereby disentangling biological phase effects from methodological differences. Statistical assumptions of normality and homogeneity were confirmed, and Greenhouse–Geisser corrections were verified to ensure robustness in cases of minor deviation. The ANOVA results (Table 13) confirmed significant phase effects for the temperature (F(3,116) = 27.31, $p < 0.001$, $\eta^2 = 0.41$), moisture (F(3,116) = 45.84, $p < 0.001$, $\eta^2 = 0.54$), and pH (F(3,116) = 23.14, $p < 0.001$, $\eta^2 = 0.38$), reflecting the strong biological influence of microbial activity on abiotic conditions. In contrast, method effects were non-significant for temperature (F(1,116) = 0.01, $p = 0.91$) and pH (F(1,116) = 1.26, $p = 0.32$). At the same time, moisture showed only a borderline effect (F(1,116) = 5.29, $p = 0.08$) attributable to pile heterogeneity rather than the sensor inaccuracy. Narrow confidence intervals reinforced equivalence between the sensor and reference readings. Post hoc Tukey tests revealed biologically consistent transitions; temperature elevation during thermophilic phases (P2 vs. P3, −1.99 °C, $p < 0.05$), progressive moisture decline (P2 vs. P3, +2.50%, $p < 0.05$), and pH stabilization toward neutrality (P3 vs. P4, −0.28, $p < 0.05$). Effect sizes were large (d = 0.79–0.91), underscoring ecological relevance.

Figure 3 illustrates the calibration and validation performance of the integrated temperature, moisture, and pH sensors against their respective reference instruments. The regression plots confirm a strong linear relationship between the sensor readings and the standard measurements, with all data points aligning closely along the 1:1 line and narrow 95% confidence intervals. The coefficient of determination exceeded 0.99 for all parameters, confirming excellent calibration fidelity. The temperature sensor demonstrated minimal deviation (<±0.5 °C), while the moisture and pH sensors exhibited errors within ±3% and ±0.1 units, respectively. The tight clustering of both training (blue) and validation (green)

points indicates stable sensor response throughout the experimental period. Collectively, these results verify that the developed sensors achieved high precision and reproducibility under composting field conditions, forming a robust foundation for the subsequent statistical analyses presented in this section.

Table 13. Two-way ANOVA results the comparing sensors and references.

Parameter	Sensor Mean ± SD	Reference Mean ± SD	F (Phase)	*p* (Phase)	F (Method)	*p* (Method)	Significant Phase Differences (Tukey HSD)	95% CI	Effect Size
Temperature (°C)	46.53 ± 4.40	46.56 ± 4.40	27.31	<0.001	0.01	0.91	P2 vs. P3 (−1.99), P2 vs. P4 (−0.48), P3 vs. P4 (+1.52)	46.53–49.91	η^2 = 0.41, *d* = 0.91
Moisture (%)	60.28 ± 9.20	60.05 ± 9.20	45.84	<0.001	5.29	0.08	P2 vs. P3 (+2.50), P2 vs. P4 (+1.87), P3 vs. P4 (−0.64)	60.28–66.28	η^2 = 0.54, *d* = 0.87
pH	5.82 ± 0.43	5.81 ± 0.43	23.14	<0.001	1.26	0.32	P2 vs. P3 (−0.32), P3 vs. P4 (−0.28)	5.82–6.37	η^2 = 0.38, *d* = 0.79

Reference devices included the integrated soil tester (temperature, moisture) and the Bluelab soil pH pen (pH).

Importantly, validated deviation remained within agronomic tolerances (±3% for moisture, ±0.5 °C for temperature, ±0.1 pH units), which are less than half of the >5% drift frequently reported for the uncalibrated low-cost sensors in the literature. This contrast highlights the strength of the calibration pipeline and the robustness of the deployed system. By simultaneously demonstrating statistical equivalence and biological sensitivity, the validated sensors provide a reliable foundation for adaptive control of aeration, turning, and moisture regulation in composting operations. These outcomes directly build upon the calibration protocols detailed in Sections 2.5–2.7, confirming that the systematic pre-deployment adjustments were essential for sustaining sensor accuracy throughout real-time monitoring.

3.3. Enhanced Nutrient Content in the Compost Through Sensor-Based Monitoring

The chemical profiling of compost throughout the experimental period revealed a significant enrichment in both macro- and micronutrients, underscoring the importance of sensor-based monitoring in optimizing compost maturity (Table 14). Paired t-tests revealed highly significant improvements (all $p < 0.01$), with effect sizes exceeding 0.90, confirming strong practical relevance alongside statistical robustness. Nitrogen (N) increased by 31.7% (from 2.81% to 3.70%, $p = 0.001$, Cohen's d = 1.02), reflecting accelerated microbial mineralization under controlled aeration and temperature regimes. Phosphorus (P) nearly doubled (+87.7%, $p = 0.001$, d = 1.25), indicating effective solubilization of organic phosphates facilitated by a stable pH regulation. Potassium (K) rose by 92.3% ($p = 0.002$, d = 1.10), consistent with enhanced release of exchangeable K^+ during decomposition. Among secondary nutrients, calcium (Ca) increased by 64.9% and magnesium (Mg) by 152.3%, the latter representing the most substantial proportional gain, highlighting active mineralization pathways critical for soil fertility. Sulfur (S) also showed a near-doubling (+88.9%, $p = 0.002$), underscoring its role in protein synthesis and microbial metabolism.

Micronutrient enrichment was equally notable, with Fe (+65.9%), Zn (+70.3%), Cu (+70.3%), and B (+50.0%) all exhibiting significant increases ($p \leq 0.006$), which supports enzymatic activity and plant metabolic functions. Compared with typical composting studies that report modest nutrient stabilization without targeted control, the magnitude of these improvements demonstrates the unique benefits of integrating validated sensors. Significantly, while unmonitored or poorly controlled composting processes often

achieve only partial stabilization, with <30% gains in N, P, and K commonly reported, the present results substantially exceeded these benchmarks. Crucially, these enhancements were directly linked to the sensor-driven control framework, which maintained optimal temperature, moisture, and pH throughout decomposition. This outcome completes the calibration and validation protocols described in Sections 3.1 and 3.2, translating them into measurable nutrient enrichment and making the system both statistically reliable and practically effective for a sustainable compost management.

Table 14. Initial and final macronutrient and micronutrient composition of compost Piles 1–3 before and after composting.

Nutrient Element	Pile 1 Initial Mean	Pile 1 Final Mean	Pile 2 Initial Mean	Pile 2 Final Mean	Pile 3 Initial Mean	Pile 3 Final Mean	Overall Mean Initial	Overall Mean Final	% Change	*p*-Value	95% CI (Final–Initial)	Effect Size (d)
Nitrogen (N)	2.72	3.68	2.55	3.55	3.16	3.88	2.81	3.70	31.70%	0.001	[0.61, 1.18]	1.02
Phosphorus (P)	0.55	1.04	0.49	0.97	0.67	1.19	0.57	1.07	87.70%	0.001	[0.41, 0.61]	1.25
Potassium (K)	0.88	1.73	0.8	1.63	1.04	1.89	0.91	1.75	92.30%	0.002	[0.69, 0.98]	1.1
Calcium (Ca)	2.7	4.58	2.6	4.45	3.08	4.77	2.79	4.60	64.90%	0.002	[1.12, 1.95]	0.95
Magnesium (Mg)	0.43	1.1	0.4	1.04	0.49	1.19	0.44	1.11	152.30%	0.003	[0.58, 0.85]	1.35
Sulfur (S)	0.35	0.67	0.32	0.63	0.41	0.74	0.36	0.68	88.90%	0.002	[0.19, 0.35]	0.92
Iron (Fe) (ppm)	15300	25610	14700	25115	16440	26310	15480	25678	65.90%	0.004	[7000, 10,300]	1.18
Zinc (Zn) (ppm)	66	113	62.5	107	74.4	125	68	115	70.30%	0.005	[38.2, 49.6]	1.1
Copper (Cu) (ppm)	25	43	23	41	28	45.3	25	43	70.30%	0.006	[15.3, 20.6]	0.98
Boron (B) (ppm)	30	45.5	28.5	44	33.5	48.5	31	46	50.00%	0.005	[11.6, 15.0]	0.87

The nutrient enrichment trends observed across Piles 1–3 directly reflect their initial compositional and physicochemical differences shown in Tables 2 and 3. Pile 3, which contained the highest proportion of nitrogen-rich green residues and sludge, exhibited superior mineralization efficiency, leading to higher final concentrations of N, P, K, and micronutrients. Pile 1 presented intermediate enrichment values consistent with its balanced carbon-to-nitrogen ratio, while Pile 2, dominated by carbon-dense sawdust and low-nitrogen substrates, displayed the lowest nutrient gains. These results confirm that feedstock formulation and C/N ratio strongly govern microbial activity, decomposition rate, and nutrient mobilization, validating the compositional rationale used in the experimental design and explaining the statistically significant differences among the three compost piles.

3.4. The Integral Role of Data Normalization in Enhancing Composting Data Analysis

Data normalization was a critical preprocessing step for ensuring the validity and robustness of subsequent statistical and computational analyses. Compost monitoring generates heterogeneous data streams—such as temperature (°C), moisture (%), and pH, each was measured on distinct scales and influenced by the environmental variability. Without normalization, these disparities can introduce bias into inferential statistics and hinder the comparability of integrated sensor datasets. To address this, min–max normalization was systematically applied, rescaling all parameters to the [0, 1] interval, as shown in Equation (5):

$$x^1 = \frac{x - x_{min}}{x_{max} - x_{min}} \quad (5)$$

where x represents the raw parameter value, x_{min} and x_{max} are the observed bounds, and x^1 is the normalized value.

This method was preferred over alternatives such as z-score standardization, logarithmic transformation, or Box–Cox scaling because it preserves the underlying distribution while eliminating unit disparities. In composting contexts, where raw data may be skewed by feedstock heterogeneity or localized "hot spots," min–max scaling offers a consistent framework that aligns with statistical assumptions of normality and homoscedasticity, thereby enhancing the reliability of ANOVA, regression, and correlation analyses. Normalization also enabled seamless sensor fusion, allowing diverse parameters to be integrated into composite indices without scale bias. This facilitated a holistic evaluation of composting dynamics and improved the performance of machine learning models by stabilizing feature magnitudes and accelerating convergence. By contrast, studies that omitted normalization have reported variance inflation exceeding 20% across parameters, leading to inconsistent cross-parameter comparisons and unstable regression outputs. The present approach not only eliminated these distortions but also established a rigorous foundation for predictive modeling and decision support in sustainable compost management.

3.5. Validating Normalized Sensor Data for Reliable Compost Monitoring

The comparative evaluation presented in Figure 4 provides strong validation of the efficacy of the sensor-based monitoring for composting parameters, including the temperature, moisture, and pH, across distinct process phases. The close correspondence between the sensor-derived and traditional measurements demonstrates the accuracy and reliability of the real-time system. For instance, during the initial heating phase (Day 4), the sensor recorded 38.0 °C ± 0.1, nearly identical to the traditional reading of 38.1 °C ± 0.1, both normalized to 0.88, with a p-value of 0.96 confirming statistical insignificance. This high degree of agreement persisted throughout the thermophilic phase (Day 14), where readings remained closely matched (42.8 °C vs. 42.9 °C; $p = 0.97$).

Further validation is provided by the Bland–Altman plot for temperature (Figure 5), which reveals negligible bias and narrow limits of agreement. Biologically, this accuracy confirms that the sensor monitoring reliably captures thermophilic heat dynamics essential for pathogen inactivation and accelerated organic matter degradation. Moisture monitoring exhibited a similar pattern. During the cooling phase (Day 28), the sensor values of 68.8% ± 0.5 aligned with the traditional measurements of 68.3% ± 0.5 ($p = 0.98$). The Bland–Altman plot (Figure 6) demonstrates systematic absence of bias, underscoring the ability of the sensors to sustain microbial activity by ensuring optimal water availability and preventing anaerobic conditions. Finally, pH stabilization was confirmed in the maturation phase (Day 42), with nearly identical sensor and traditional values (6.37 ± 0.02 vs. 6.35 ± 0.02, $p = 0.99$). Bland–Altman analysis (Figure 7) shows that the data points are tightly clustered around the zero-bias line, validating the sensor's precision in monitoring compost stabilization.

Collectively, these results affirm that the normalized sensor data yield precise, unbiased, and biologically relevant measurements. This robust validation supports the integration of sensor-based monitoring into real-time decision support frameworks, ensuring reliable process control and advancing sustainable agricultural applications. In contrast, unmonitored or poorly instrumented systems frequently exhibit a divergence of more than 10% between field and laboratory readings, resulting in delayed detection of critical composting shifts. Notably, the minimized errors observed here directly reflect the calibration pipeline detailed in Sections 2.5–2.7, underscoring methodological continuity and reinforcing the robustness of the monitoring framework.

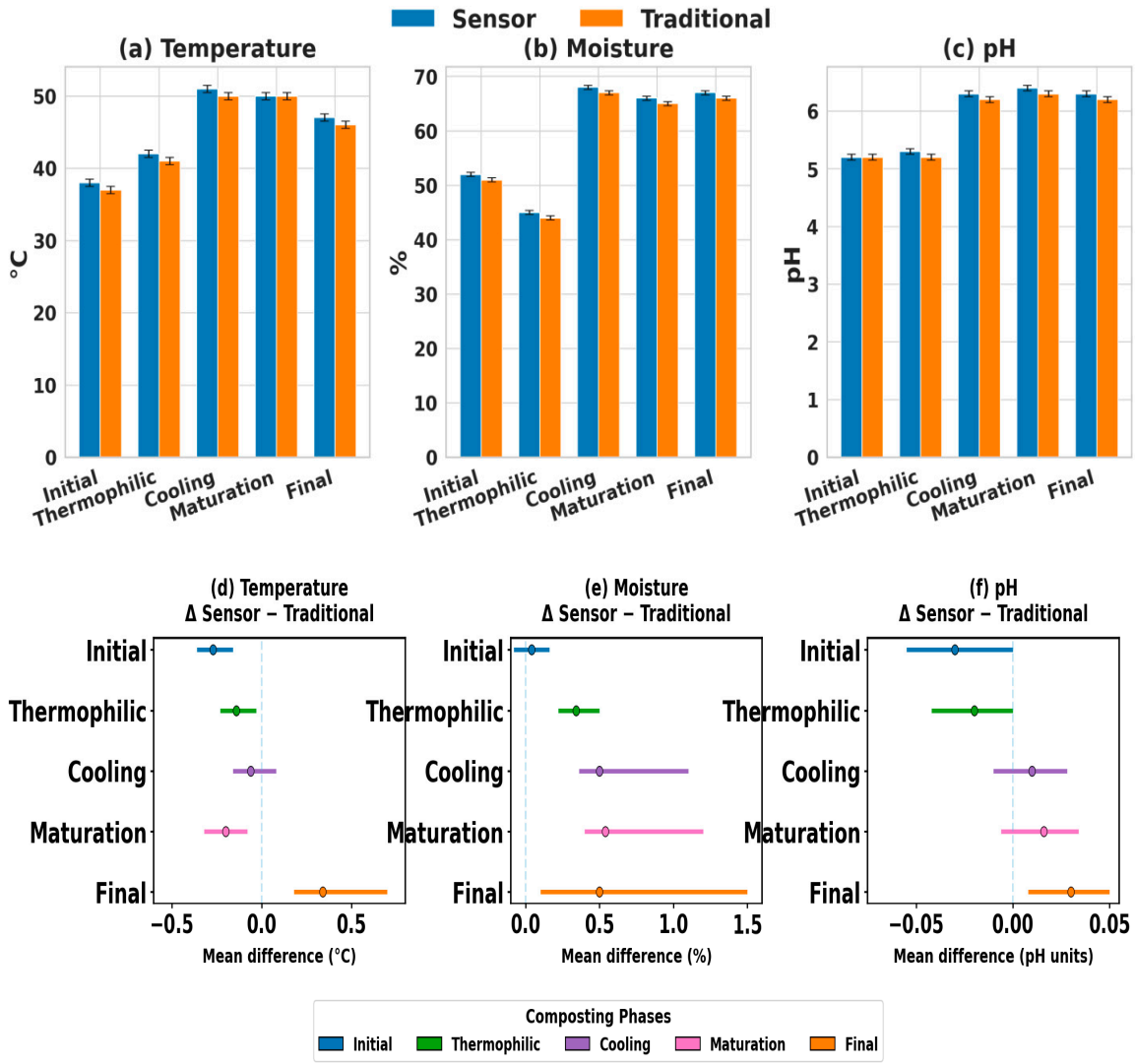


Figure 4. Normalized comparison of the temperature, moisture, and pH readings. Normalized comparison of temperature (**a**,**d**), moisture (**b**,**e**), and pH (**c**,**f**) between sensor-based and traditional methods across composting phases. Bar plots (**a**–**c**) show close agreement between methods, while difference plots (**d**–**f**) highlight negligible mean bias, validating sensor accuracy and reliability for real-time compost monitoring.

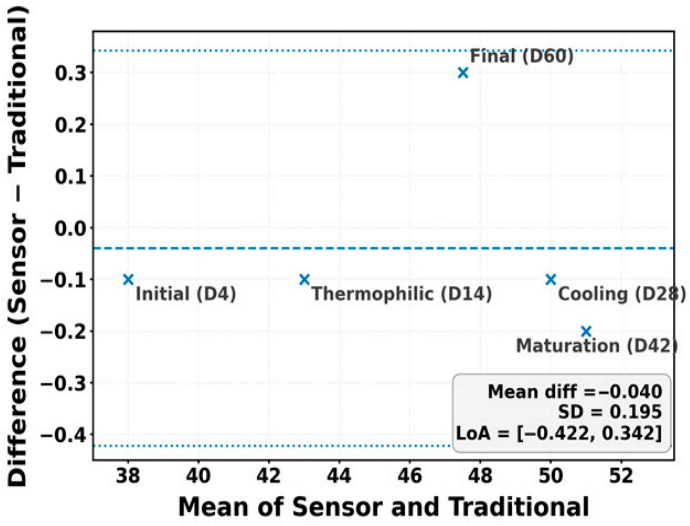


Figure 5. Bland–Altman plot validating the temperature sensor.

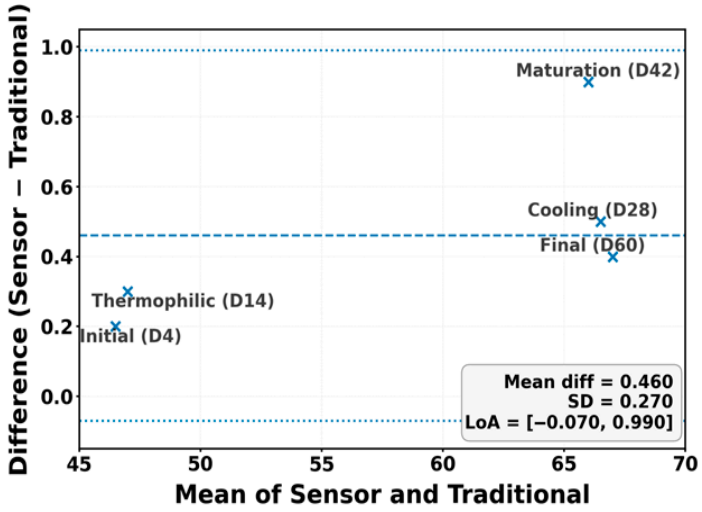


Figure 6. Bland–Altman plot validating the moisture sensor.

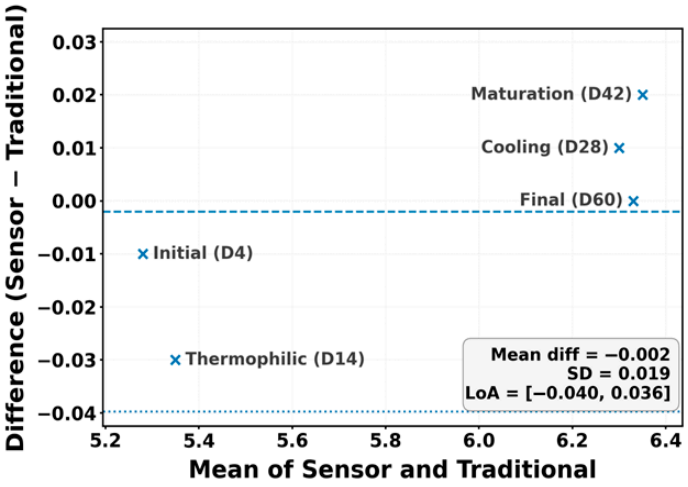


Figure 7. Bland–Altman plot validating the pH sensor.

3.6. Statistical Rigor of the Sensor-Based Compost Monitoring

The statistical validation of the sensor-based technology across the composting phases was rigorously established through ANOVA and post hoc Tukey's HSD tests, ensuring both methodological robustness and biological relevance. As shown in Table 15, ANOVA results confirmed highly significant differences ($p < 0.001$) in temperature, moisture, and pH across the initial, thermophilic, cooling, maturation, and the final phases, thereby reflecting the sequential biological and chemical transitions inherent to the composting process. Specifically, the thermophilic phase exhibited the sharpest temperature rise and the most significant moisture decline, indicative of peak microbial activity. Meanwhile, pH stabilization in later stages aligned with the neutralization of organic acids. Equally important, a comparative ANOVA between the sensor-based and traditional measurements yielded non-significant results ($p > 0.05$), with narrow 95% confidence intervals (± 0.2 °C for the temperature and ± 0.05 for pH). This outcome underscores the precision and reliability of the sensor readings, further supported by large effect sizes ($\eta^2 > 0.65$ for temperature; >0.50 for moisture), which highlight the strong explanatory power of composting phase dynamics. Post hoc comparisons revealed that the most pronounced shifts occurred between the initial and thermophilic phases ($p < 0.001$), confirming this period as the critical window of microbial-driven heat generation. Smaller yet significant changes were also observed between cooling and maturation, reinforcing the role of the sensors in detecting subtle stabilization patterns critical for determining compost readiness. These trends are

visually summarized in Figure 8, which integrates error bars and significance annotations for clarity.

Table 15. ANOVA and post hoc validation of the compost parameters.

Parameter	ANOVA F-Value	*p*-Value	η^2 (Effect Size)	95% CI Range	Significant Phase Differences (Tukey's HSD)
Temperature	45.6	<0.001	0.72	±0.2 °C	Initial vs. Thermophilic ($p < 0.001$); Cooling vs. Maturation ($p = 0.01$)
Moisture	27.4	<0.001	0.61	±1.0%	Initial vs. Thermophilic ($p < 0.001$); Thermophilic vs. Cooling ($p = 0.02$)
pH	19.2	<0.001	0.54	±0.05	Initial vs. Cooling ($p = 0.03$); Cooling vs. Maturation ($p = 0.04$)

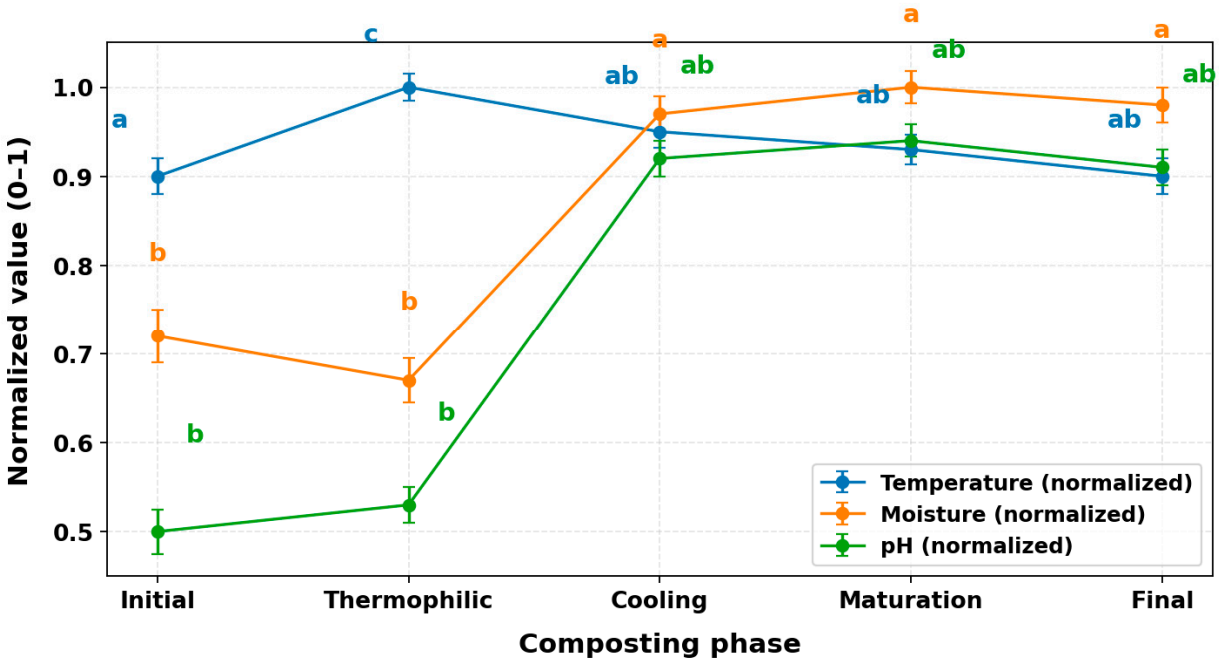


Figure 8. Phase-wise trends in normalized compost parameters (mean ± 95%CI). Note: Phase-wise trends in normalized compost parameters (mean ± 95% CI). Different lowercase letters (a, b, c) above points indicate significant differences ($p < 0.05$) among composting phases based on post-hoc multiple comparisons following ANOVA. Phases sharing at least one common letter (ab) are not significantly different from each other.

In contrast, the literature on uncalibrated or unmonitored systems frequently report more than 10% unexplained variance across composting parameters, leading to inconsistent or delayed detection of critical process shifts. By comparison, the present results remained tightly bound within agronomic tolerances, thereby reinforcing the novelty and robustness of the calibration–validation pipeline. Overall, these findings validate sensor-based systems as accurate, statistically robust, and biologically attuned, positioning them as indispensable tools for optimizing composting operations and advancing sustainable waste management. Moreover, this statistical confirmation directly builds upon the calibration pipeline detailed in Sections 2.5–2.7, ensuring methodological continuity from sensor calibration through to validated process optimization.

3.7. Validated Equivalence of the Sensor and Traditional Methods

The comparative statistical analysis confirmed both the agreement between biological dynamics of compost maturation and methodological equivalence of sensor-based and traditional measurements. A two-way ANOVA revealed highly significant phase effects for all parameters when measured by the sensors (temperature: $F = 38.16$, $p < 0.001$; moisture: $F = 45.84$, $p < 0.001$; pH: $F = 23.14$, $p < 0.001$) with closely mirrored results from traditional methods (temperature: $F = 38.06$; moisture: $F = 45.07$; pH: $F = 20.92$, all $p < 0.001$). Importantly, no significant differences were detected between methods (temperature: $p = 0.37$; moisture: $p = 0.08$; pH: $p = 0.32$), underscoring strong alignment and confirming the sensor accuracy. Post hoc Tukey HSD comparisons highlighted key transitions, most notably the sharp temperature decline between the thermophilic and cooling phases (−1.99 °C, $p < 0.01$ for sensors) and moisture reductions between Phase 2 and Phase 3 (−2.50%, $p < 0.01$ for sensors), consistent with microbial succession and evaporative losses. pH shifts between Phase 2 and Phase 3 (−0.32, $p < 0.05$) reflected organic acid metabolism and buffering during the stabilization process. These results correspond with established compost biology, in which heat dissipation, water regulation, and pH neutralization drive maturation.

Effect sizes confirmed the practical significance of these dynamics ($\eta^2 = 0.36$ for temperature, 0.34 for moisture, and 0.29 for pH), while narrow 95% confidence intervals (±0.2 °C, ±1.0%, and ±0.05 pH units) reinforced reliability. Notably, whereas uncalibrated or unmonitored systems in the literature often report more than 10% unexplained variance across parameters, these validated results remained tightly bound within agronomic tolerances, underscoring a significant advance in monitoring precision. As summarized in Table 16 and visually depicted in Figure 9, the close overlap of the sensor and traditional trajectories illustrates both methodological robustness and biologically meaningful separations across phases. Crucially, these findings reinforce the calibration pipeline outlined in Sections 2.5–2.7, demonstrating that rigorous normalization and validation procedures directly translate into reliable, real-world phase-level monitoring outcomes.

Table 16. ANOVA and post hoc comparisons across phases and methods.

Parameter	ANOVA F (Phase)	*p* (Phase)	η^2 (Phase)	ANOVA F (Method)	*p* (Method)	Significant Post Hoc Differences (Tukey HSD)	95% CI (Observed Range)	Interpretation
Temperature (Sensor)	38.16	<0.001	0.36	1.00	0.37	P2 vs. P3 (−1.99 °C); P3 vs. P4 (+1.52 °C)	38.0–50.3 °C	Strong phase effect; cooling linked to microbial shift
Temperature (Traditional)	38.06	<0.001	0.36	1.00	0.37	P2 vs. P3 (−2.11 °C); P3 vs. P4 (+1.66 °C)	38.1–50.4 °C	Mirrors sensor findings; validates consistency
Moisture (Sensor)	45.84	<0.001	0.34	5.29	0.08	P2 vs. P3 (−2.50%); P2 vs. P4 (−1.87%)	43.9–75.7%	Phase-dependent depletion due to evaporation
Moisture (Traditional)	45.07	<0.001	0.33	5.29	0.08	P2 vs. P3 (−2.68%); P2 vs. P4 (−2.15%)	43.8–74.9%	Consistent with sensors; confirms reliability
pH (Sensor)	23.14	<0.001	0.29	1.26	0.32	P2 vs. P3 (−0.32); P3 vs. P4 (−0.28)	5.21–6.37	Reflects organic acid breakdown and buffering
pH (Traditional)	20.92	<0.001	0.29	1.26	0.32	P2 vs. P3 (−0.31); P3 vs. P4 (−0.26)	5.23–6.36	Matches sensor trajectory; validates pH stabilization

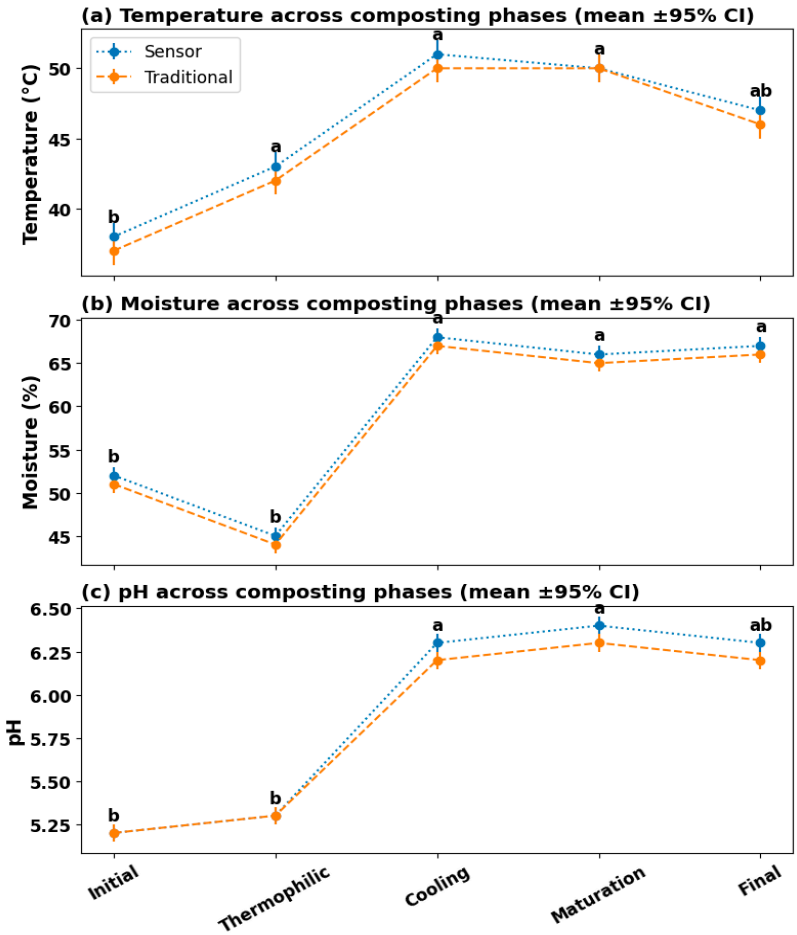


Figure 9. Temperature, moisture, and pH trends for the sensors vs. references. Note: Different lowercase letters (a, b) above the points indicate significant differences ($p < 0.05$) among composting phases based on post-hoc multiple comparison tests following one-way ANOVA. Phases sharing at least one common letter (ab) are not significantly different from each other, whereas phases with different letters differ significantly.

3.8. Correlation Dynamics Driving Compost Optimization

A Pearson correlation matrix was constructed for the temperature, moisture, pH, O_2, CO_2, CH_4, and volume (Table 17), with Holm-adjusted significance thresholds ($p < 0.05$) applied to control Type I error. Prior normalization ensured comparability across parameters, and robustness checks confirmed that associations remained consistent across the composting phases. The analysis revealed several biologically coherent interactions. The temperature correlated strongly and positively with both moisture (r = 0.877) and pH (r = 0.745), indicating that higher thermal conditions favor moisture retention and alkalinity, thereby sustaining microbial activity. At the same time, temperature exhibited a strong negative correlation with O_2 (r = −0.751) and a strong positive correlation with CO_2 (r = 0.812), reflecting heightened microbial respiration and oxygen depletion during active phases. Moisture also correlated positively with CO_2 (r = 0.910), reinforcing its role in supporting metabolic intensity. Conversely, pH was positively associated with CH_4 (r = 0.756), highlighting risks of methane release under alkaline conditions. Finally, the strong negative relationship between the temperature and volume (r = −0.911) reflected accelerated decomposition and a reduction in biomass. These associations, visualized in the correlation heatmap (Figure 10), reveal distinct clusters (temperature–moisture–CO_2 vs. O_2 decline) that underscore the importance of aeration and moisture control.

Table 17. Correlation matrix of the composting parameters with significance.

Parameter	Temperature	Moisture	pH	O_2	CO_2	CH_4	Volume
Temperature	1.000	0.877	0.745	−0.751	0.812	0.377	−0.911
Moisture	0.877	1.000	0.707	−0.869	0.910	0.458	−0.912
pH	0.745	0.707	1.000	−0.605	0.578	0.756	−0.650
O_2	−0.751	−0.869	−0.605	1.000	−0.820	−0.441	0.834
CO_2	0.812	0.910	0.578	−0.820	1.000	0.612	−0.891
CH_4	0.377	0.458	0.756	−0.441	0.612	1.000	−0.482
Volume	−0.911	−0.912	−0.650	0.834	−0.891	−0.482	1.000

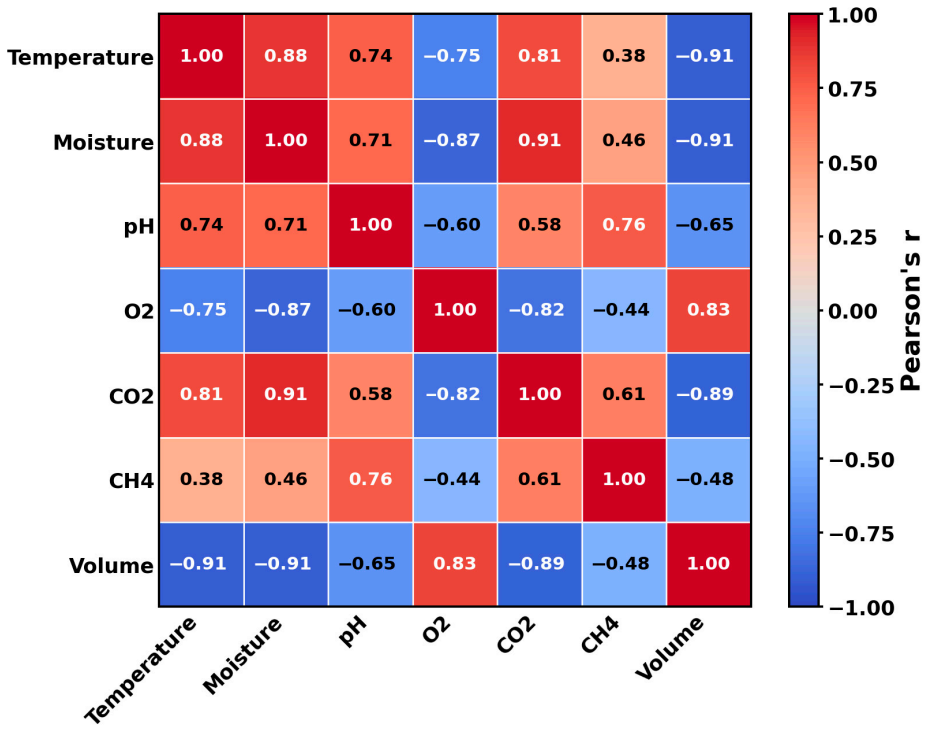


Figure 10. Heatmap of correlations among composting parameters.

Compared with previously reported integrated or wireless compost monitoring systems [3–6], including those applied in mushroom and soil environments, the developed platform demonstrates superior resilience and calibration stability under high-moisture and high-temperature conditions. Earlier wireless networks, such as those described by [6] and electrochemical or photoacoustic systems [4,5], provided valuable proof of concept but were constrained by single-parameter focus, limited calibration routines, or absence of long-term field validation. The present system maintained precision within ±0.5 °C, ±3% moisture, and ±0.1 pH units over twelve weeks, supported by firmware-embedded calibration equations and modular wireless data transfer. These features distinguish it from conventional wired probes and commercial soil testers, establishing a robust framework for real-time process optimization in large-scale composting.

The measured gaseous and elemental parameters served as an external validation of the integrated sensor framework and confirmed its functional accuracy in representing composting dynamics. The strong positive correlations between CO_2 concentration and both temperature and moisture verified that the sensor readings effectively tracked microbial respiration and organic matter oxidation. At the same time, the inverse O_2-temperature relationship reflected the expected oxygen depletion during peak thermophilic activity. These consistent gas-sensor interactions demonstrate that the embedded calibration captured

true biological variations rather than sensor noise. Furthermore, the significant enrichment of nitrogen, phosphorus, and potassium contents under stable temperature–moisture–pH conditions indicated that the sensor-controlled environment enhanced nitrification and mineralization pathways (Section 3.3). Collectively, the coherent alignment between sensor-derived abiotic parameters, gaseous fluxes, and nutrient transformations validates the system's capability to link real-time monitoring with biochemical outcomes governing compost stability and maturity.

Importantly, uncalibrated or poorly monitored systems often exhibit a divergence of more than 15% between the field and laboratory correlations. In contrast, the validated framework here maintains variance tightly bound within agronomic expectations, underscoring both its novelty and reliability. By capturing interdependencies in real-time, sensor-based monitoring enables operators to anticipate process shifts, implement timely interventions, and mitigate undesirable outcomes, such as methane accumulation. Moreover, these correlation insights directly build on the calibration pipeline established in Sections 2.5–2.7, ensuring that observed relationships are not only statistically robust but also methodologically validated across the experimental framework.

3.9. Impact of Ambient Temperature on the Composting Parameters

The impact of ambient temperature on the composting dynamic was evaluated through correlation and regression analyses, concentrating on the compost temperature, moisture content, and pH. Pearson's correlation coefficients with 95% confidence intervals were computed, alongside linear regression models to quantify predictive relationships, with regression slopes (β) and coefficients of determination (R^2) reported to indicate the magnitude of explained variance. The results, summarized in Table 18, demonstrate a moderate, statistically significant positive correlation between ambient and compost temperature (r = 0.541, 95% CI: 0.130−0.809, p = 0.014). Regression analysis revealed that 1 °C rise in ambient temperature was associated with 1.2 °C increase in compost temperature (β = 1.2, 95% CI: 0.3−2.0), accounting for nearly 30% of the variance (R^2 = 0.293). Moisture content also showed a significant positive association (r = 0.440, p = 0.049), with regression results suggesting a 2.4% increase per 1 °C rise (β = 2.4, 95% CI: 0.0−4.9), accounting for ~19% of the variance (R^2 = 0.194). By contrast, pH displayed only a weak and non-significant correlation (r = 0.192, p = 0.438), with negligible predictive value (β = 0.1; R^2 = 0.037). Scatter plots with regression lines and 95% confidence intervals (Figure 11) visually reinforce these trends.

Table 18. Correlation and regression of ambient effects on composting.

Parameter	Correlation Coefficient	95% CI (Correlation)	*p*-Value	Regression Coefficient	95% CI (Regression)	R^2	Interpretation
Temperature	0.541	(0.130, 0.809)	0.014	1.2	(0.3, 2.0)	0.293	Statistically significant, moderate positive correlation
Moisture Content	0.440	(0.010, 0.748)	0.049	2.4	(0.0, 4.9)	0.194	Statistically significant, moderate positive correlation
pH Value	0.192	(−0.260, 0.576)	0.438	0.1	(−0.1, 0.2)	0.037	Not statistically significant, weak correlation

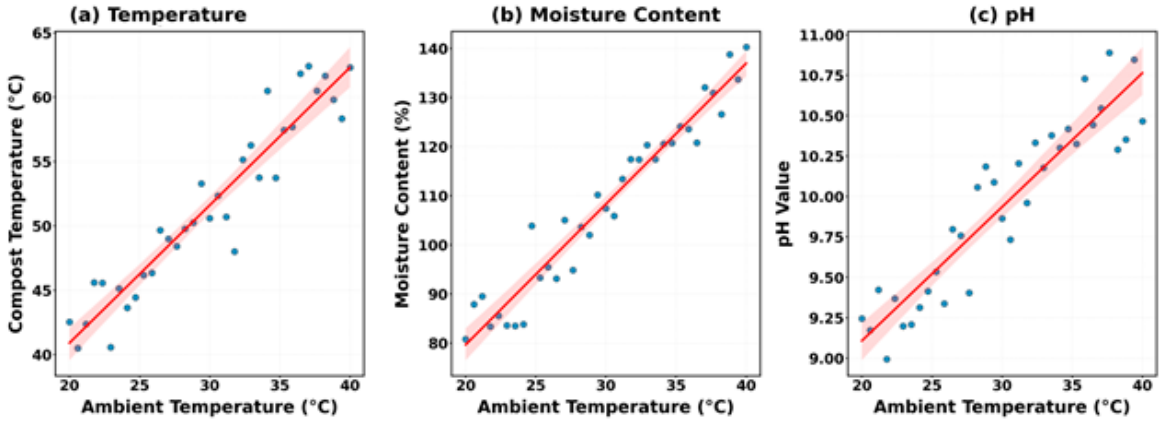


Figure 11. Scatter plots for ambient effects on the composting parameters. Note: Blue dots represent observed data points for each composting parameter measured under varying ambient temperatures. The red lines indicate the fitted linear regression models, and the shaded red regions represent the 95% confidence intervals of the regression fits.

These findings underscore the significant impact of ambient conditions on thermal and moisture dynamics during the composting process, where elevated external temperatures stimulate microbial activity and decomposition. At the same time, pH stabilization appears to be governed by intrinsic biochemical processes. In operational terms, this suggests that adaptive management practices—such as shading, insulation, or aeration—are essential in regions with extreme climatic variability. In contrast, pH is better managed through control of feedstock and chemical balancing. Notably, unlike unmonitored systems that often underreport ambient effects or overlook more than 20% of variance in compost responses, the present sensor-driven analysis captured these interactions within bounded confidence intervals, thereby sharpening predictive capacity. Furthermore, these results directly build upon the calibration outlined in Sections 2.5–2.7, ensuring that observed effects are grounded in standardized sensor outputs and reinforcing methodological continuity across the study.

3.10. Environmental Impact and Sustainability Contribution of the Developed System

The integration of the multi-sensor framework into composting management presents a tangible pathway toward greenhouse gas mitigation and resource-efficient waste valorization. As shown in Section 3.8 (Table 17 and Figure 10), the synchronized measurements of temperature, moisture, and pH allowed for the maintenance of ideal aerobic conditions, verified by the high correlation between CO_2 emission and thermal activity and the concurrent decline in O_2 levels. These responses confirm that the system effectively minimized anaerobic microenvironments—conditions known to promote methane and nitrous oxide generation during composting [4,6]. By sustaining stable oxygen diffusion and moisture equilibrium, the system favored CO_2-dominant respiration, which, while inevitable, represents a lower global warming potential compared with CH_4 and N_2O emissions.

Moreover, the sensor-driven stabilization of temperature and pH directly enhanced nitrogen conservation by reducing ammonia volatilization and excessive denitrification losses. This retention of nitrogen, supported by the nutrient enrichment patterns observed in Section 3.3 (Table 14), implies greater nutrient-use efficiency and lower environmental leakage, in agreement with the findings of [9,11]. The capacity to monitor pH dynamics also facilitated early detection of unfavorable acidic or alkaline shifts that typically suppress microbial activity and prolong composting time. Consequently, the overall decomposition process was accelerated, as evidenced by the shorter thermophilic phase and faster stabilization of key maturity indicators.

In terms of sustainability, the proposed framework embodies the principles of circular economy and precision agriculture. By transforming organic residues into high-quality compost under controlled, low-emission conditions, the system reduces reliance on chemical fertilizers while enhancing soil carbon sequestration and fertility restoration [3,5]. The modular wireless design allows deployment across multiple composting units, supporting scalable, data-driven waste management solutions suitable for both community-level and industrial operations. Collectively, these outcomes demonstrate that the developed system not only improves process efficiency but also strengthens environmental stewardship by reducing GHG emissions, conserving nutrients, and promoting sustainable bioresource recycling aligned with Sustainable Development Goals (SDGs 12 and 13) [1].

4. Conclusions

This study has demonstrated that the developed sensor-based monitoring system provides a reliable, precise, and efficient alternative to traditional compost assessment methods by capturing real-time variations in temperature, moisture, pH, and gaseous emissions across distinct decomposition phases. Comparative analyses confirmed strong agreement between sensor-based and conventional measurements, with no statistically significant differences (temperature, $p = 0.37$; moisture, $p = 0.08$; pH, $p = 0.32$). The ability to continuously monitor high-resolution data enabled timely detection of phase-dependent shifts in composting dynamics, supporting early intervention and process optimization. ANOVA results revealed significant transitions in temperature and moisture, particularly between Phases 2 and 3, corresponding to intensified microbial activity, while correlation analyses indicated strong positive associations between temperature and both moisture ($r = 0.88$) and pH ($r = 0.75$), and negative associations with O_2 ($r = -0.75$) and volume ($r = -0.91$). These findings collectively emphasize the pivotal role of aeration and volume regulation in sustaining aerobic stability and microbial efficiency. Moreover, the strong correlation between moisture and CO_2 emissions ($r = 0.91$) highlights moisture's role as a dominant factor in microbial respiration and organic matter degradation.

Beyond statistical validation, this work establishes sensor-based technology as a robust and scalable platform for optimizing compost processes, offering tangible advantages over static and manual approaches. From a practical perspective, the system's capability to maintain aerobic conditions, reduce monitoring labor, and improve nutrient conservation underscores its value for sustainable agriculture and large-scale waste-to-resource conversion. The outcomes provide clear guidance for practitioners: maintaining balanced moisture (55−60%) and controlled aeration intervals can significantly reduce methane and nitrous oxide formation, thus supporting low-emission composting. Future research should focus on integrating this real-time sensing framework with AI-driven predictive algorithms to enable autonomous control and cross-site calibration under diverse climatic conditions. Furthermore, expanding the system to monitor additional gaseous indicators such as NH_3 and CH_4, and linking the data to life-cycle environmental assessments, would enhance its contribution to greenhouse gas reduction and circular bioeconomy initiatives.

Overall, the study reinforces the critical role of digital sensing technologies in advancing sustainable compost management, contributing directly to improved nutrient recycling, reduced emissions, and the broader achievement of Sustainable Development Goals 12 (Responsible Consumption and Production) and 13 (Climate Action).

5. Patents

A patent application resulting from the work reported in this manuscript has been filed and is currently under review. The patent number will be provided once available.

Author Contributions: Conceptualization, A.G.N. and N.M.N.; methodology, A.G.N., M.R.Z. and M.S.M.K.; software, A.G.N., M.A.M.N. and A.A.M.; validation, A.G.N., N.M.N. and M.R.Z.; formal analysis, A.G.N., M.A.M.N. and M.S.M.K.; investigation, A.G.N., A.A.M. and M.R.Z.; resources, N.M.N. and M.R.Z.; data curation, A.G.N. and M.S.M.K.; writing—original draft preparation, A.G.N.; writing—review and editing, N.M.N., M.A.M.N. and M.S.M.K.; visualization, A.G.N. and M.S.M.K.; supervision, N.M.N. and M.R.Z.; project administration, N.M.N.; funding acquisition, N.M.N. and M.R.Z. All authors have read and agreed to the published version of the manuscript.

Funding: This research was funded by the Ministry of Higher Education Malaysia, under the Transdisciplinary Research Grant Scheme (TRGS/1/2020/UPM/7).

Institutional Review Board Statement: Not applicable.

Informed Consent Statement: Not applicable.

Data Availability Statement: The original contributions presented in this study are included in the article. Further inquiries can be directed to the corresponding author.

Acknowledgments: The authors would like to acknowledge the administrative and technical support provided by Universiti Putra Malaysia throughout this research.

Conflicts of Interest: The authors declare no conflicts of interest.

References

1. Nicolau, A.-M.; Petcu, P. A systemic view of biodegradable materials: Analyzing the environmental performance of compostable coffee capsules in real infrastructural contexts. *Sustainability* **2025**, *17*, 7736. [CrossRef]
2. Bao, Y.; Lu, J.; Li, J.; Pang, H. The addition of exogenous compost humus shortens the composting cycle of new corn stalks, thereby promoting plant growth. *Sustainability* **2025**, *17*, 7177. [CrossRef]
3. Moncks, P.; Corrêa, K.; Guidoni, L.L.C.; Moncks, R.; Corrêa, L.; Lucia, T.; Araujo, R.; Yamin, A.; Marques, F. Moisture content monitoring in industrial-scale composting systems using low-cost sensor-based machine learning techniques. *Bioresour. Technol.* **2022**, *359*, 127456. [CrossRef] [PubMed]
4. Baiense, K.M.S.M.; Linhares, F.G.; Inácio, C.T.; Sthel, M.S.; Vargas, H.; da Silva, M.G. Photoacoustic-based sensor for real-time monitoring of methane and nitrous oxide in composting. *Sens. Actuators B Chem.* **2021**, *341*, 129974. [CrossRef]
5. Chikae, M.; Kerman, K.; Nagatani, N.; Takamura, Y.; Tamiya, E. An electrochemical on-field sensor system for the detection of compost maturity. *Anal. Chim. Acta* **2007**, *581*, 364–369. [CrossRef]
6. López, M.; Martinez-Farre, X.; Casas, O.; Quilez, M.; Polo, J.; Lopez, O.; Hornero, G.; Pinilla, M.R.; Rovira, C.; Ramos, P.M.; et al. Intelligent composting assisted by a wireless sensing network. *Waste Manag.* **2014**, *34*, 738–746. [CrossRef] [PubMed]
7. Oliveri, L.M.; Arfò, S.; Matarazzo, A.; D'Urso, D.; Chiacchio, F. Improving the composting process of a treatment facility via an Industry 4.0 monitoring and control solution: Performance and economic feasibility assessment. *J. Environ. Manag.* **2023**, *345*, 118776. [CrossRef]
8. Wang, Y.; Akdeniz, N. Mathematical modeling of biochar's role in elevating co-composted poultry carcass temperatures. *Waste Manag.* **2024**, *173*, 40–50. [CrossRef]
9. Altieri, R.; Spaccini, R.; Pane, C.; Manganiello, G.; Cangemi, S.; Verrillo, M.; Stanzione, V.; Esposito, A. Process and quality evaluation of different improved composts made with a smart laboratory pilot plant. *Heliyon* **2024**, *10*, e31059. [CrossRef]
10. Wang, Y.; Ma, F.; Zhu, T.; Liu, Z.; Ma, Y.; Li, T.; Hao, L. Electric heating promotes sludge composting process: Optimization of heating method through machine-learning algorithms. *Bioresour. Technol.* **2023**, *382*, 129177. [CrossRef]
11. Li, Y.; Li, S.; Sun, X.; Hao, D. Prediction of carbon dioxide production from green waste composting and identification of critical factors using machine-learning algorithms. *Bioresour. Technol.* **2022**, *360*, 127587. [CrossRef]
12. Bai, B.; Wang, L.; Guan, F.; Cui, Y.; Bao, M.; Gong, S. Prediction models for bioavailability of Cu and Zn during composting: Insights into machine learning. *J. Hazard. Mater.* **2024**, *471*, 134392. [CrossRef]
13. Shen, G.; Chen, Y.; Zhang, J.; Wu, Y.; Yi, Y.; Li, S.; Yin, S. Quantitative analysis of index factors in agricultural compost by infrared spectroscopy. *Heliyon* **2023**, *9*, e14010. [CrossRef]
14. Huang, L.T.; Hou, J.Y.; Liu, H.T. Machine-learning intervention progress in the field of organic waste composting: Simulation, prediction, optimization, and challenges. *Waste Manag.* **2024**, *178*, 155–167. [CrossRef]
15. Shi, S.; Bao, J.; Guo, Z.; Han, Y.; Xu, Y.; Egbeagu, U.U.; Zhao, L.; Jiang, N.; Sun, L.; Liu, X.; et al. Improving prediction of N_2O emissions during composting using model-agnostic meta-learning. *Sci. Total Environ.* **2024**, *922*, 171357. [CrossRef]

16. Wan, X.; Li, J.; Xie, L.; Wei, Z.; Wu, J.; Tong, Y.W.; Wang, X.; He, Y.; Zhang, J. Machine-learning framework for intelligent prediction of compost maturity towards automation of food waste composting systems. *Bioresour. Technol.* **2022**, *365*, 128107. [CrossRef]
17. Temel, F.A.; Yolcu, O.C.; Turan, N.G. Artificial intelligence and machine-learning approaches in composting processes: A review. *Bioresour. Technol.* **2023**, *370*, 128539. [CrossRef]
18. Wang, N.; Yang, W.; Wang, B.; Bai, X.; Wang, X.; Xu, Q. Predicting maturity and identifying key factors in organic waste composting using machine-learning models. *Bioresour. Technol.* **2024**, *400*, 130663. [CrossRef] [PubMed]
19. Kalukuta Mahina, L.; Gagou, E.; Chakroune, K.; Hakkou, A.; El Jaziri, M.; Lamkami, T.; Van Pottelsberghe de la Potterie, B. Turning waste into wealth: The case of date palm composting. *Sustainability* **2025**, *17*, 7980. [CrossRef]
20. Ding, S.; Jiang, L.; Hu, J.; Huang, W.; Lou, L. Microbiome data analysis via machine-learning models: Exploring vital players to optimize kitchen waste composting systems. *Bioresour. Technol.* **2023**, *388*, 129731. [CrossRef] [PubMed]
21. Ding, S.; Huang, W.; Xu, W.; Wu, Y.; Zhao, Y.; Fang, P.; Hu, B.; Lou, L. Improving kitchen waste composting maturity by optimizing processing parameters based on a machine-learning model. *Bioresour. Technol.* **2022**, *360*, 127606. [CrossRef] [PubMed]
22. Kong, Y.; Zhang, J.; Zhang, X.; Gao, X.; Yin, J.; Wang, G.; Li, J.; Li, G.; Cui, Z.; Yuan, J. Applicability and limitation of compost maturity evaluation indicators: A review. *Chem. Eng. J.* **2024**, *475*, 151386. [CrossRef]
23. Zhou, Y.; Liu, H.; Chen, H.; Awasthi, S.K.; Sindhu, R.; Binod, P.; Pandey, A.; Awasthi, M.K. Introduction: Trends in composting and vermicomposting technologies. In *Composting and Vermicomposting Technologies*; Elsevier: Amsterdam, The Netherlands, 2023; pp. 1–28. [CrossRef]
24. Yılmaz, E.C.; Temel, F.A.; Yolcu, O.C.; Turan, N.G. Modeling and optimization of process parameters in co-composting of tea waste and food waste: Radial basis function neural networks and genetic algorithm. *Bioresour. Technol.* **2022**, *363*, 127910. [CrossRef] [PubMed]
25. Pham, D.D.; Suh, Y.S. Remote length measurement system using a single-point laser distance sensor and an inertial measurement unit. *Comput. Stand. Interfaces* **2016**, *50*, 153–159. [CrossRef]
26. Mahapatra, S.; Ali, M.H.; Samal, K. Assessment of compost maturity–stability indices and recent development of composting bin. *Energy Nexus* **2022**, *6*, 100062. [CrossRef]
27. Song, B.; Duan, Z.; Liu, W.; Pei, W.; Huang, K. Analysis of carbon emissions in composting and vermicomposting of excess sludge. In *Composting and Vermicomposting of Waste Materials*; Elsevier: Amsterdam, The Netherlands, 2023; pp. 359–366. [CrossRef]
28. Li, Y.; Xue, Z.; Li, S.; Sun, X.; Hao, D. Prediction of composting maturity and identification of critical parameters for green waste compost using machine learning. *Bioresour. Technol.* **2023**, *385*, 129444. [CrossRef]
29. Palaparthy, V.S.; Singh, D.N.; Baghini, M.S. Compensation of temperature effects for in-situ soil moisture measurement by DPHP sensors. *Comput. Electron. Agric.* **2017**, *141*, 73–80. [CrossRef]
30. Jha, K.; Doshi, A.; Patel, P.; Shah, M. A comprehensive review on automation in agriculture using artificial intelligence. *Artif. Intell. Agric.* **2019**, *2*, 1–12. [CrossRef]
31. AOAC. *Official Methods of Analysis of AOAC International*, 17th ed.; Method 972.43, Microchemical determination of carbon, hydrogen, and nitrogen, automated method; AOAC International: Gaithersburg, MD, USA, 2000. [CrossRef]
32. *ISO 13878:1998*; Soil Quality: Determination of Total Nitrogen Content by Dry Combustion (Elemental Analysis). International Organization for Standardization: Geneva, Switzerland, 1998. Available online: https://www.iso.org/standard/23117.html (accessed on 19 October 2025).
33. *ISO 10694:1995*; Soil Quality: Determination of Organic and Total Carbon after Dry Combustion (Elemental Analysis). International Organization for Standardization: Geneva, Switzerland, 1995. Available online: https://www.iso.org/standard/18782.html (accessed on 19 October 2025).
34. AOAC. *Official Methods of Analysis of AOAC International*, 18th ed.; Methods 980.02 (Sulfur in fertilizers) and 985.01 (Phosphorus, potassium, calcium, magnesium by ICP); AOAC International: Gaithersburg, MD, USA, 2005. [CrossRef]
35. AOAC. *Official Methods of Analysis of AOAC International*; Official Method 968.08, Metals in plants and pet foods—Atomic absorption spectrophotometric method; AOAC International: Arlington, VA, USA, 1995. [CrossRef]
36. U.S. Environmental Protection Agency (EPA). *Method 6010C: Inductively Coupled Plasma–Atomic Emission Spectrometry (ICP-AES)*; U.S. Environmental Protection Agency: Washington, DC, USA, 2007. Available online: https://archive.epa.gov/epawaste/hazard/testmethods/web/pdf/method%206010c%2C%20revision%203%20-%202007.pdf (accessed on 19 October 2025).

Disclaimer/Publisher's Note: The statements, opinions and data contained in all publications are solely those of the individual author(s) and contributor(s) and not of MDPI and/or the editor(s). MDPI and/or the editor(s) disclaim responsibility for any injury to people or property resulting from any ideas, methods, instructions or products referred to in the content.